



## Article

# Wildfire Probability Mapping: Bivariate vs. Multivariate Statistics

Abolfazl Jaafari <sup>1</sup>, Davood Mafi-Gholami <sup>2</sup>, Binh Thai Pham <sup>3,\*</sup> and Dieu Tien Bui <sup>4,\*</sup>

<sup>1</sup> Research Institute of Forests and Rangelands, Agricultural Research, Education, and Extension Organization (AREEO), Tehran 13185-116, Iran; jaafari@rifra.ac.ir

<sup>2</sup> Department of Forest Sciences, Faculty of Natural Resources and Earth Sciences, Shaherkord University, Shaherkord 8818634141, Iran; d.mafigholami@nres.sku.ac.ir

<sup>3</sup> Institute of Research and Development, Duy Tan University, Da Nang 550000, Vietnam

<sup>4</sup> Geographic Information System Group, Department of Business and IT, University of South-Eastern Norway, Gullbringvegen 36, N-3800 Bø i Telemark, Norway

\* Correspondence: binhpt@utt.edu.vn (B.T.P.); Dieu.T.Bui@usn.no (D.T.B.)

Received: 20 January 2019; Accepted: 7 March 2019; Published: 13 March 2019



**Abstract:** Wildfires are one of the most common natural hazards worldwide. Here, we compared the capability of bivariate and multivariate models for the prediction of spatially explicit wildfire probability across a fire-prone landscape in the Zagros ecoregion, Iran. Dempster–Shafer-based evidential belief function (EBF) and the multivariate logistic regression (LR) were applied to a spatial dataset that represents 132 fire events from the period of 2007–2014 and twelve explanatory variables (altitude, aspect, slope degree, topographic wetness index (TWI), annual temperature, and rainfall, wind effect, land use, normalized difference vegetation index (NDVI), and distance to roads, rivers, and residential areas). While the EBF model successfully characterized each variable class by four probability mass functions in terms of wildfire probabilities, the LR model identified the variables that have a major impact on the probability of fire occurrence. Two distribution maps of wildfire probability were developed based upon the results of each model. In an ensemble modeling perspective, we combined the two probability maps. The results were verified and compared by the receiver operating characteristic (ROC) and the Wilcoxon Signed-Rank Test. The results showed that although an improved predictive accuracy ( $AUC = 0.864$ ) can be achieved via an ensemble modeling of bivariate and multivariate statistics, the models fail to individually provide a satisfactory prediction of wildfire probability ( $EBF_{AUC} = 0.701$ ;  $LR_{AUC} = 0.728$ ). From these results, we recommend the employment of ensemble modeling approaches for different wildfire-prone landscapes.

**Keywords:** Zagros ecoregion; evidential belief function; logistic regression; ensemble modeling

## 1. Introduction

Wildland fires are complex phenomena with a large number of uncertain and highly unpredictable driving factors that still remain undiscovered [1,2]. In recent years, a surge in the loss of lives, property, and biodiversity caused by wildfires occurred worldwide [3,4]. Some estimations indicate that the future climate change and its effects on rainfall patterns and drought occurrences will further exacerbate wildfires in many parts of the world [5,6], which, in turn, places strong demands on the managers to adopt wildfire risk mitigation strategies in the face of future climate change. In an effort to mitigate the effects of the wildfires, managers delineate fire-prone landscapes for allocating suppression resources and firefighting efforts [7], often based on the fire management systems [8]. Various fire management and prevention systems have been suggested and developed in different countries such as USA, Canada, Spain, Portugal, and Australia [9,10] that have originated from

attempts to satisfy a growing demand for fire prevention in the fire-prone landscapes [7]. These systems are usually based on a predictive model which aims at providing near-time wildfire predictions up to 10–15 years into the future [7,11].

Given the investment of resources and time required to suppress wildfires, efficient and adaptable techniques are needed to rapidly estimate the likelihood of fire occurrence. The first extensive works on predicting wildfire probability date back to Chuvieco and Congalton [12] in Spain and De Vliegheer [13] in Greece, which were significantly elaborated by recent works [14–16], demonstrating that the future wildfires tend to occur under similar local conditions that caused them in the past.

Wildfire predictive modeling is typically performed in the following five steps [2,7,11,14–16]: (1) Detecting and documenting historical fire events; (2) identifying a set of wildfire influencing factors; (3) seeking the potential relationships between the influencing factors and the historical fires; (4) elaborating a spatially explicit distribution map of wildfire probability; and (5) assessing the reliability of the probability map and its utility for predicting the location of future fires. Over the past decades, researchers mostly focused on step three of this methodology and evaluated various models in an explicitly spatial way to fully explore the pattern of wildfire occurrences in response to different geo-environmental factors [2,7,14–16]. Apart from the machine learning techniques that have emerged in recent years [14,15], bivariate and multivariate methods have always been the most commonly used modeling approaches [7,17,18]. While the machine learning techniques (e.g., artificial neural networks, neuro-fuzzy, support vector machines, and decision trees) often enable the modelers/managers to achieve a high level of predictive accuracy, their application requires a profound knowledge of programming to adequately tune several hyper-parameters that control the model performance [16]. On the other hand, the bivariate (e.g., frequency ratio, weight of evidence, evidential belief function, statistical index, and certainty factor) and multivariate (e.g., linear and logistic regressions) methods can easily be performed with in an Excel spreadsheet and the other user-friendly interfaces and represent a straightforward analytic framework [7,17–20]. These methods have been numerically formulated to be easily used in different environmental settings and adapted to include updated datasets with low complexity and computation costs. Based on the spatial relationships between input data, these models predict the probability of occurrence (positive) or non-occurrence (negative) of a fire with probability  $P(+) = 1 - P(-)$  [7,11,14].

However, these models operate on different mathematical concepts (bivariate vs. multivariate) that do not necessarily lead to the same performance in different environmental settings. For example, Pourtaghi et al. [18] mapped forest fire susceptibility using the frequency ratio model and achieved a predictive accuracy of 79.85%. Pourghasemi [17] used the evidential belief function and regression logistic for mapping forest fire probability and reported predictive accuracies of 74.30 and 81.93%, respectively. Jaafari et al. [7] and Hong et al. [19] employed the weight of evidence model and demonstrated the capability of this model with predictive accuracies of 80.39% and 82.02%, respectively. Nami et al. [20] used the evidential belief function and successfully mapped the wildfire probability with a predictive accuracy of 81.03%. Most recently, Hong et al. [21] compared the weight of evidence and regression logistic and reported predictive accuracies of 85.4 and 79.1%, respectively. These reviews of the literature clearly indicate that there is no single best model that can be effectively used in all fire-prone landscapes.

Additionally, however, some researchers combined bivariate and multivariate methods toward a more accurate predictive model and often achieved a significantly improved overall predictive accuracy compared to the single models, as an integrated ensemble model offers higher capability in the organization and description of data [16]. For example, in the context of landslide modeling, Umar et al. [22] and Chen et al. [23] reported improved predictive accuracies for the integrated frequency ratio-logistic regression and weight of evidence-logistic regression models compared to the single frequency ratio and weight of evidence models. To date, however, such a modeling approach has been rarely applied for wildfire prediction [24].

In Iran, based on a report issued by the Forests, Range, and Watershed Management Organization (FRWO), about 6000 ha of forests have been devastated by fires in 2017 alone. Particularly, the Zagros ecoregion in Western Iran is highly affected by frequent wildfires due to its favorable climatic, biophysical, and socioeconomic conditions [20]. Investigations of influencing factors and the production of probability maps have been rarely performed for this highly susceptible ecoregion [7,25]. In this study, we sought to build on these efforts by using and comparing evidential belief function (EBF) and linear regression (LR) models to map wildfire probability in a fire-prone landscape of the Zagros. The modeling approach adopted in this study is motivated by a desire to better explain the mechanisms responsible for wildfire occurrences in the Zagros eco-region and to understand the nature and capability of different models for treating the uncertainty inhered in the spatial explicit modeling of wildfires.

## 2. Study Area

This study was conducted in the central highlands of the Zagros ecoregion, Western Iran, located between 31°9' N to 32°48' N latitude and 49°28' E to 51°25' E longitude (WGS 1984/UTM zone 39N) (Figure 1). The study area is a 16,532 km<sup>2</sup> extent characterized by vegetation conditions ranging from grasslands to scatter forests dominated by Persian oak (*Quercus persica*) [7]. Topography varies widely across the area (slope = 0–84°; altitude = 783–4178 m) and significantly affects the local climate conditions. Annual rainfall varies from 1400 mm in the Northwest to 250 mm in the East and Southeast. Historically, winter and spring have been the wettest seasons of the year. The mean annual temperature ranges from 5 °C in the central parts to 16 °C in the Western parts, with an average of 10 °C. Most of the wildfires that occur in this area are caused due to decreased rainfall, drought occurrences, anthropogenic phenomena, or combinations thereof. Despite the frequency of wildfires in this portion of the Zagros ecoregion, few studies have investigated the wildfire probability in this area [14].

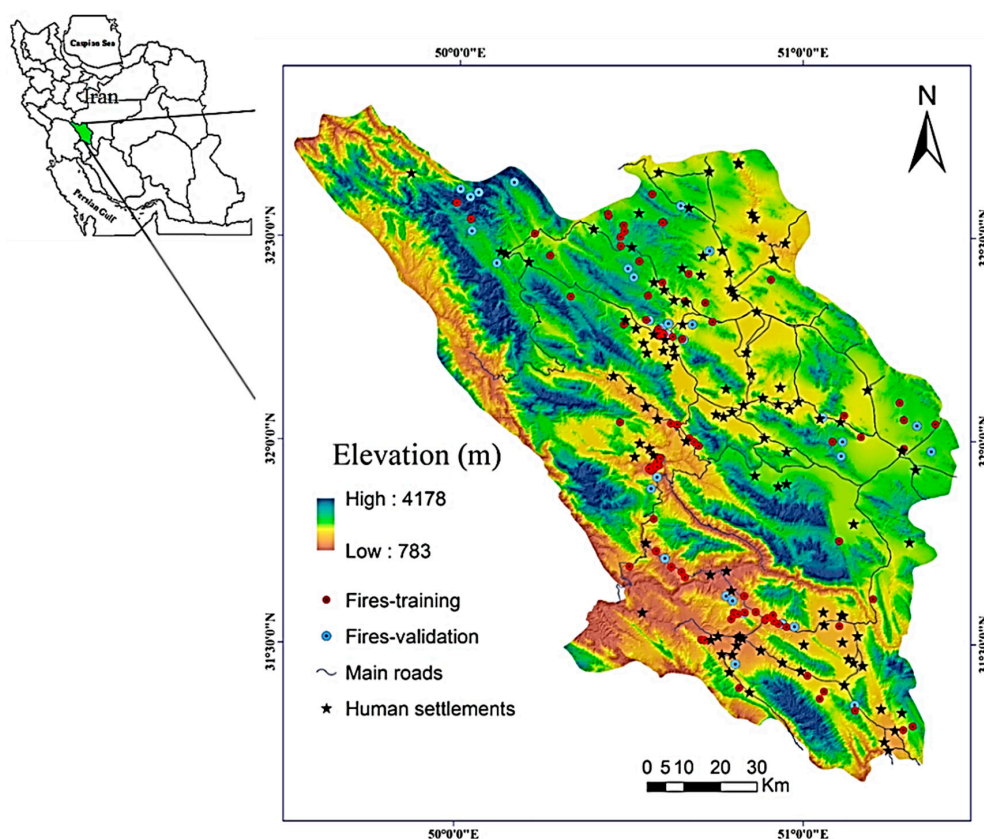


Figure 1. Location of the study area and historical fires.

### 3. Methodology

The step by step workflow of the methodology adopted in this study is shown in Figure 2 and includes (1) compiling a wildfire inventory map and a set of the independent/explanatory variables, (2) multicollinearity assessment, (3) predictive modeling of wildfire occurrences using the EBF and LR models, (4) validating and comparing the models, (5) producing wildfire probability maps, and (6) developing a probability map via an ensemble modeling approach.

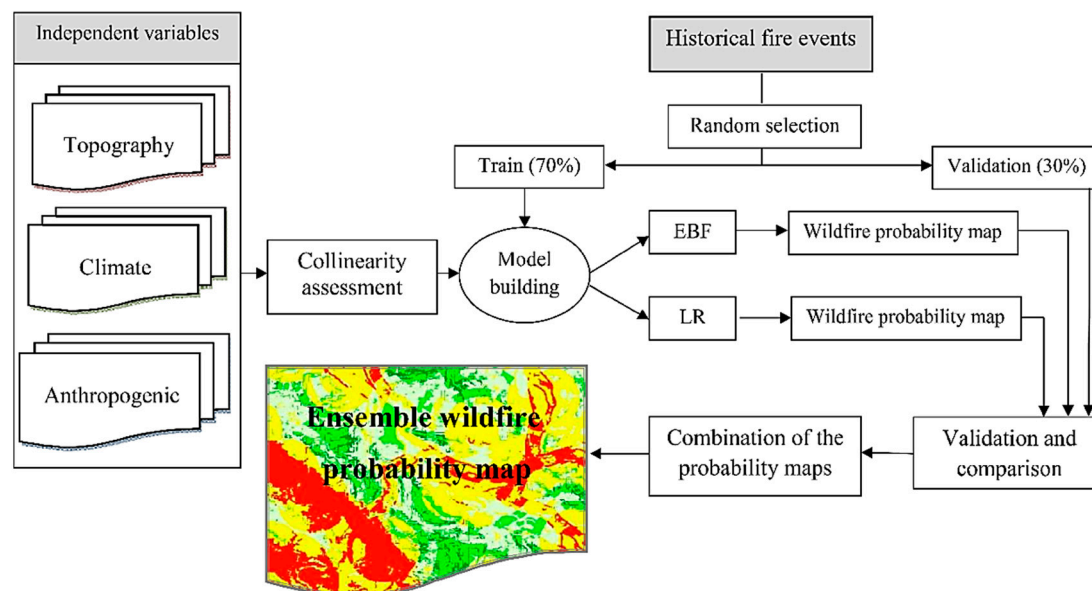


Figure 2. Workflow of the methodology adopted in this study.

#### 3.1. Wildfire Inventory

An inventory of historical wildfires is the main basis for the statistical analyses of wildfire probabilities and can be conducted in different ways ranging from field surveys to interpretation of satellite imagery [15,20]. To prepare an inventory map of the wildfires that have occurred in the study area, we first referred to the historical archives to identify the spatial locations of the burnt areas in the recent past. We then used MODIS hot spot products (<http://earthdata.nasa.gov/firms>) and conducted several field surveys in various parts of the study area to verify the information of historical archives and produce a more reliable inventory map. Finally, we ended up with an inventory map that consists of occurrence records of 137 fires for the period of 2007–2014 (Figure 1).

Following previous works [2,7,14–21], we randomly sub-divided the wildfire locations into training and validation data subsets. The training dataset included 70% of the wildfires (1096 pixels) and the validation dataset included the remaining 30% of the wildfires (470 pixels).

#### 3.2. Independent Variables

An important task in wildfire predictive modeling is to identify the set of variables that carry complementary information. To adequately account for all local characteristics of the study area, twelve independent variables that have been frequently used in the wildfire literature were considered: Altitude, aspect, slope degree, topographic wetness index (TWI), annual temperature, and rainfall, wind effect, land use, normalized difference vegetation index (NDVI), and distance to roads, rivers, and populated areas. We refer the interested reader to the corresponding literature [7,11,14–21,24] for the information on the significance of these variables on wildfire occurrence and their utility for predictive modeling of future fires. To produce a topographic dataset describing altitude, aspect, slope, and TWI, we used a Digital Elevation Model (DEM) at 30-meter resolution. We processed the information obtained from the Meteorological Organization of the National Cartographic Center



of Iran to extract the maps of rainfall, temperature, wind effect, and distance to roads, rivers, and residential areas. Furthermore, we generated the land use and NDVI maps of the study area using Landsat-8 OLI 30 m (<http://earthexplorer.usgs.gov>). Finally, we categorized each explanatory variable into several classes based on the previous works [14–21,24,25] and local conditions of our study landscape (Figure 3).

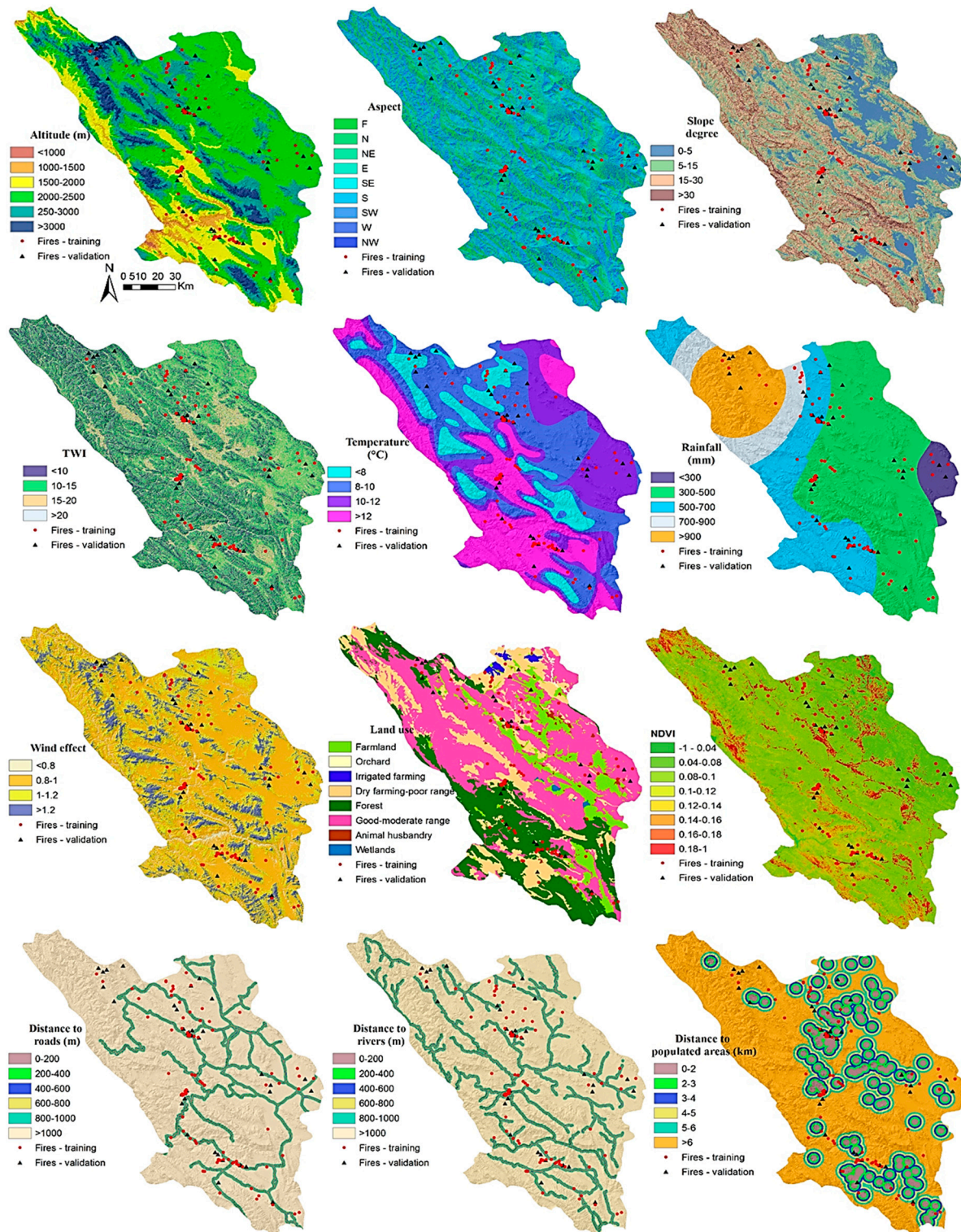


Figure 3. Independent/explanatory variables used in this study.

### 3.3. Multicollinearity Assessment

Most of the bivariate and multivariate techniques are sensitive to the inclusion of the collinear variables, as these intercorrelated variables can significantly reduce the accuracy of the model [7]. Thus, before model building, the highly collinear variables should be identified and excluded from further procedures [7–16]. To examine possible collinearity among the variables used in this study, we computed the variance inflation factor (VIF) and tolerance and checked their critical values for all variables. VIF > 5 or tolerance < 0.2 indicate a multicollinearity problem and the variable(s) labeled with these values should be removed.

### 3.4. Evidential Belief Function (EBF)

The evidential belief function (EBF) model is a quantitative data-driven approach based on the Dempster–Shafer theory [26]. Originally developed by Dempster [27,28], the method was further improved by Shafer [29] for dealing with uncertain, incomplete, and manifold information from multiple sources using various combination rules to get an overall view of the problem [20]. This model consists of four main probability mass functions, including degree of belief (Bel), degree of disbelief (Dis), degree of uncertainty (Unc), and degree of plausibility (Pls), which are scaled in the range of 0–1 [30,31]. While Bel and Pls indicate the lower and upper probability of the generalized Bayesian theory, their difference (Unc) represents the doubt that the evidence supports a proposition [32]. Disfunction refers to a degree of disbelief in evidence with respect to the proposition [33] and is equal to  $1 - \text{Pls}$  (or  $1 - \text{Unc} - \text{Bel}$ ). Therefore,  $\text{Bel} + \text{Unc} + \text{Dis}$  for evidence regarding any proposition is always equal to 1 (i.e., the maximum probability) [31,33]. In the context of wildfire probability modeling, these relationships can be given by:

$$\text{Bel}_{C_{ij}} = \frac{W_{C_{ij}D}}{\sum_{j=1}^m W_{C_{ij}D}}, \quad (1)$$

$$W_{C_{ij}D} = \frac{N(C_{ij} \cap D) / N(C_{ij})}{N(D) - (N(C_{ij} \cap D)) / (N(T) - N(C_{ij}))}, \quad (2)$$

$$\text{Dis}_{C_{ij}} = \frac{W_{C_{ij}\bar{D}}}{\sum_{j=1}^m W_{C_{ij}\bar{D}}}, \quad (3)$$

$$W_{C_{ij}\bar{D}} = \frac{N(C_{ij} \cap D) / N(C_{ij})}{N(T) - N(D) - [(N(C_{ij}) - N(C_{ij} \cap D)) / (N(T) - N(C_{ij}))]}, \quad (4)$$

$$\text{Unc} = [1 - (\text{Bel}_{C_{ij}}) - (\text{Dis}_{C_{ij}})], \quad (5)$$

$$\text{Pls} = [1 - (\text{Dis}_{C_{ij}})], \quad (6)$$

where  $\text{Bel}_{C_{ij}}$  is the belief value,  $\text{Dis}_{C_{ij}}$  is the disbelief value,  $N(C_{ij} \cap D)$  is the density of fire pixels in class  $D$ ,  $N(C_{ij})$  is the total number of fire pixels in the landscape,  $N(D)$  is the number of pixels of class  $D$ , and  $N(T)$  is the total number of pixels in the landscape. A GIS-based wildfire probability modeling using the EBF model can be broken down into four main steps [20]: (1) Linking the historical fire events to the explanatory variables; (2) calculating weights for each variable class; (3) combining the multi-class weights of all variables to produce an index map for each mass function; and (4) developing a spatially explicit map of wildfire probability by combining the four maps of the mass functions.

### 3.5. Logistic Regression

As the most popular multivariate statistical analysis method for the prediction of different types of natural hazards [34], logistic regression (LR) is capable of exploring the spatial relationship between an event (dependent variable) and an array of independent variables to elucidate the underlying pattern of the occurrence of the event [34]. Since wildfire modeling is typically formulated as a binary problem, LR builds a linear relationship between the dependent variable and independent variables based on the presence (1) or absence (0) of fire. In this case, the model can be given as:

$$y = \alpha + b_{1 \times 1} + b_{2 \times 2} + \dots + b_{n \times n}, \quad (7)$$

$$P_j = \frac{1}{1 + e^{-y}} \quad (8)$$

where  $y$  is the probability of occurrence (1) or non-occurrence (0) of fire,  $\alpha$  is the intercept of the model,  $b_i$  ( $i = 0, 1, 2, \dots, n$ ) represents the model coefficients,  $x_i$  ( $i = 0, 1, 2, \dots, n$ ) donates the set of independent variables, and  $P_j$  varies between 0 and 1 and is the probability of fire occurrence in each pixel of the research landscape. The application of the LR model enables us to identify the most prominent variables that best explain the spatial pattern of wildfire probability within the landscape. All LR calculations were performed using the SPSS software and were then transferred to ArcGIS software.

### 3.6. Ensemble Modeling

To increase our chance of obtaining a more accurate estimate of wildfire probabilities, we followed an ensemble modeling approach recommended in the literature [35] and combined the two probability maps produced by the EBF and LR models, resulting in a single probability map that benefited from the advantages of both EBF and LR models that alleviated some of the limitations of the basic models. To do so, we used the raster calculator tool of the ArcGIS software and performed a simple raster overlay. This operation resulted in combining characteristics for EBF and LR maps into a single probability map.

### 3.7. Validation and Comparison

The goodness-of-fit and predictive capability of the modeling approaches adopted in this study were evaluated employing the receiver operating characteristic (ROC) curve and its two components, i.e., sensitivity and specificity, that calculated the success rate and prediction rate and their associated area under the curve (AUC). The philosophy and mathematical formulation of this method have been fully presented in the corresponding literature [14–21]. In summary, the sensitivity (i.e., probability of detection) answers the question of what fraction of the observed fire pixels are correctly classified, and its perfect value is 1; specificity (i.e., negative predictive value) answers the question of what fraction of the non-fire pixels are correctly classified, and its perfect value is 1. The ROC of the training dataset yields the success rate of the model and measures the goodness-of-fit of the model. The ROC of the validation dataset yields the prediction rate of the model and indicates how well or poorly the model predicts the future events [7,14–21]. In terms of the AUC value, the values of <0.6 indicate a poor, 0.6–0.7 a moderate, 0.7–0.8 a good, 0.8–0.9 a very good, and >0.9 an excellent model performance [36,37].

To statistically compare the performance of the models, a pairwise comparison between the probability indices extracted from each probability map was performed. This comparative analysis was conducted using the Wilcoxon Signed-Rank Test (WSRT) [38], where the null hypothesis assumes the performance of the models at the significance level of  $p = 0.05$  is the same. The  $-1.96 < z\text{-value} > 1.96$  indicates that the  $p$ -value is less than 0.05 and rejects the null hypothesis.



## 4. Results and Discussion

### 4.1. Multicollinearity Assessment

Our approach was to check and then to adequately select the predictive variables with the highest predictive utility to build the models. Careful multicollinearity assessment is required to confidently include the optimal subset of variables that make the greatest contribution to the likelihood of landslide occurrence [7,14,21]. In this study, the results of the multicollinearity assessment among the variables showed that no variable exceeded the critical values of VIF > 5 and TOL < 0.1 (Figure 4). Thus, we retained all variables in the analysis and model building [7,14].

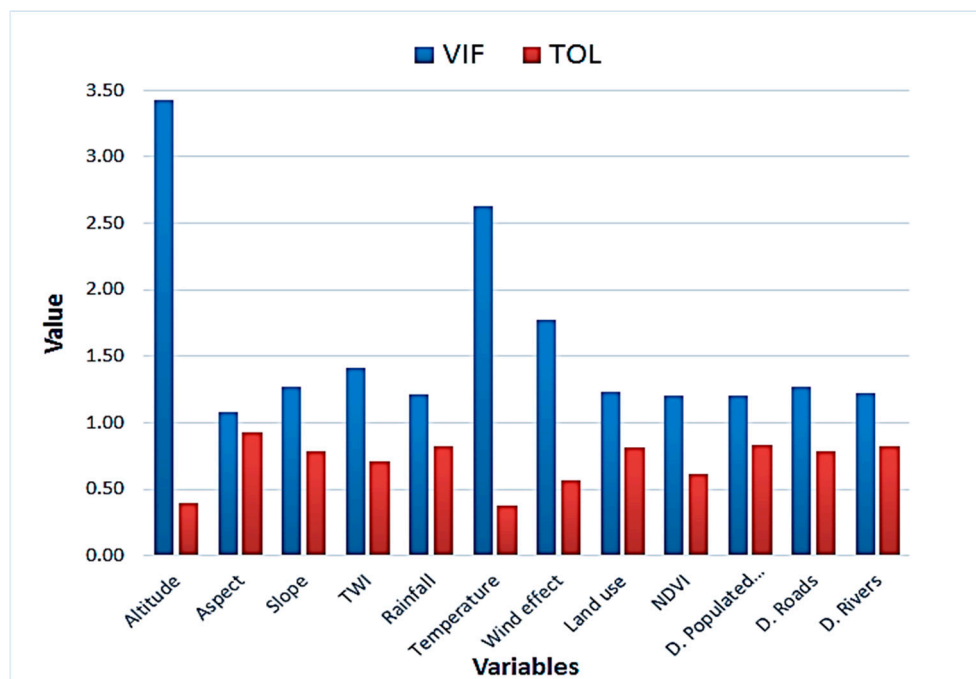


Figure 4. The multicollinearity diagnosis statistics for the variables.

### 4.2. Model Results

All classes of the twelve explanatory variables used in this study were characterized by four probability mass functions, i.e., Bel, Dis, Unc, and Pls, that indicate the level of correlation between each variable class and the probability of fire occurrences (Table 1). Applying these four sets of values, four multi-class weighted maps for each variable were developed which were separately overlaid and numerically added to develop an index map of wildfire probability for each probability mass function (Figure 5). The spatial distribution of wildfire probability under each mass function is interpreted regarding the physiography [20] and the local characteristics of the study area. In our study area, higher degrees of Bel and Pls are associated with the road networks and forested areas, while lower degrees correspond to human settlements and associated infrastructure. Whereas this is due to recreational activities along the roads and high fuel loads in the forested areas [2], low fuel load as well as fire suppression strategies protect urbanization areas against seasonal fire events [7,21]. In addition, a higher probability of fire occurrence is seen in parts of the study area that have higher degrees of Bel and lower degrees of Dis values. The Unc map is an uncertainty quantification index and provides insights into the uncertainty of the results [20]. In spatially explicit modeling, a possible source of uncertainty is the spatial heterogeneity [21]. Such a problem happens when the value of a variable at one pixel is different from its neighborhood pixels and can usually considerably limit the reliability of the interpretations made upon the modeling procedure.



**Table 1.** The spatial relationship between each predictor variable and wildfires extracted by using the evidential belief function (EBF) model.

Variable	Class	EBF Probability Mass Functions				Variable	Class	EBF Probability Mass Functions			
		Bel	Dis	Unc	Pls			Bel	Dis	Unc	Pls
Altitude (m)	0–1000	0.00	0.25	0.75	0.75	Wind effect	<0.8	0.47	0.25	0.28	0.75
	1000–1500	0.29	0.25	0.46	0.75		0.8–1	0.31	0.23	0.46	0.77
	1500–2000	0.54	0.20	0.26	0.80		1–1.2	0.26	0.26	0.47	0.74
	2000–2500	0.28	0.26	0.46	0.74		>1.2	0.22	0.26	0.52	0.74
	2500–3000	0.18	0.28	0.54	0.72						
	>3000	0.04	0.27	0.69	0.73	Land use	L1	0.11	0.27	0.61	0.73
Aspect	F	0.21	0.26	0.53	0.74		L2	0.00	0.25	0.75	0.75
	N	0.27	0.25	0.48	0.75		L3	0.45	0.25	0.30	0.75
	NE	0.29	0.25	0.46	0.75		L4	0.41	0.23	0.36	0.77
	E	0.26	0.25	0.49	0.75		L5	0.37	0.23	0.40	0.77
	SE	0.36	0.24	0.40	0.76		L6	0.24	0.29	0.48	0.71
	S	0.25	0.26	0.49	0.74		L7	0.00	0.25	0.75	0.75
	SW	0.36	0.24	0.40	0.76		L8	0.00	0.25	0.75	0.75
	W	0.30	0.25	0.44	0.75						
	NW	0.24	0.26	0.51	0.74	NDVI	−1–0.04	0.21	0.26	0.53	0.74
Slope degree	0–5	0.23	0.27	0.50	0.73		0.04–0.08	0.27	0.25	0.48	0.75
	5–15	0.39	0.21	0.40	0.79		0.08–0.1	0.29	0.25	0.46	0.75
	15–30	0.34	0.23	0.43	0.77		0.1–0.12	0.26	0.25	0.49	0.75
	>30	0.04	0.29	0.67	0.71		0.12–0.14	0.36	0.24	0.40	0.76
							0.14–0.16	0.25	0.26	0.49	0.74
TWI	<10	0.29	0.25	0.46	0.75		0.16–0.18	0.36	0.24	0.40	0.76
	10–15	0.31	0.22	0.46	0.78		0.18–1	0.30	0.25	0.44	0.75
	15–20	0.23	0.26	0.50	0.74	Distance to roads	0–200	0.71	0.24	0.05	0.76
	>20	0.11	0.26	0.64	0.74		200–400	0.71	0.24	0.05	0.76
Temperature (°C)	<8	0.25	0.26	0.49	0.74		400–600	0.65	0.24	0.10	0.76
	8–10	0.20	0.29	0.51	0.71		600–800	0.97	0.23	−0.21	0.77
	10–12	0.26	0.26	0.48	0.74		800–1000	0.33	0.25	0.41	0.75
	>12	0.43	0.20	0.37	0.80		>1000	0.22	0.60	0.18	0.40
Rainfall (mm)	<300	0.30	0.25	0.45	0.75	Distance to rivers	0–200	0.31	0.25	0.44	0.75
	300–500	0.24	0.29	0.47	0.71		200–400	0.21	0.26	0.54	0.74
	500–700	0.50	0.19	0.31	0.81		400–600	0.22	0.26	0.53	0.74
	700–900	0.21	0.26	0.53	0.74		600–800	0.57	0.24	0.19	0.76
							800–1000	0.22	0.25	0.52	0.75
Distance to populated areas							>1000				
						Distance to populated areas	0–2	0.62	0.23	0.15	0.77
							2–3	0.44	0.24	0.32	0.76
							3–4	0.55	0.23	0.22	0.77
							4–5	0.22	0.26	0.52	0.74
							5–6	0.38	0.24	0.37	0.76
							>6	0.18	0.39	0.43	0.61

The final EBF map of wildfire probability was developed by integrating the four mass probability maps and was reclassified into different probability levels representing the likelihoods of wildfire occurrence across the study landscape (Figure 6). Visually, it is evident that the high and very high levels of wildfire probability are highly associated with the road networks and forested areas. These results are in close agreement with those who reported a positive association between human activities and increased probability of fire occurrence [2,7]. However, if the EBF map is compared to the uncertainty map (Figure 5), it is evident that the areas with high uncertainty correspond

to very low and low probability classes, although several fires have occurred in these portions of the landscape. These results motivated us to consider an ensemble approach for treating the uncertainty of the EBF model.

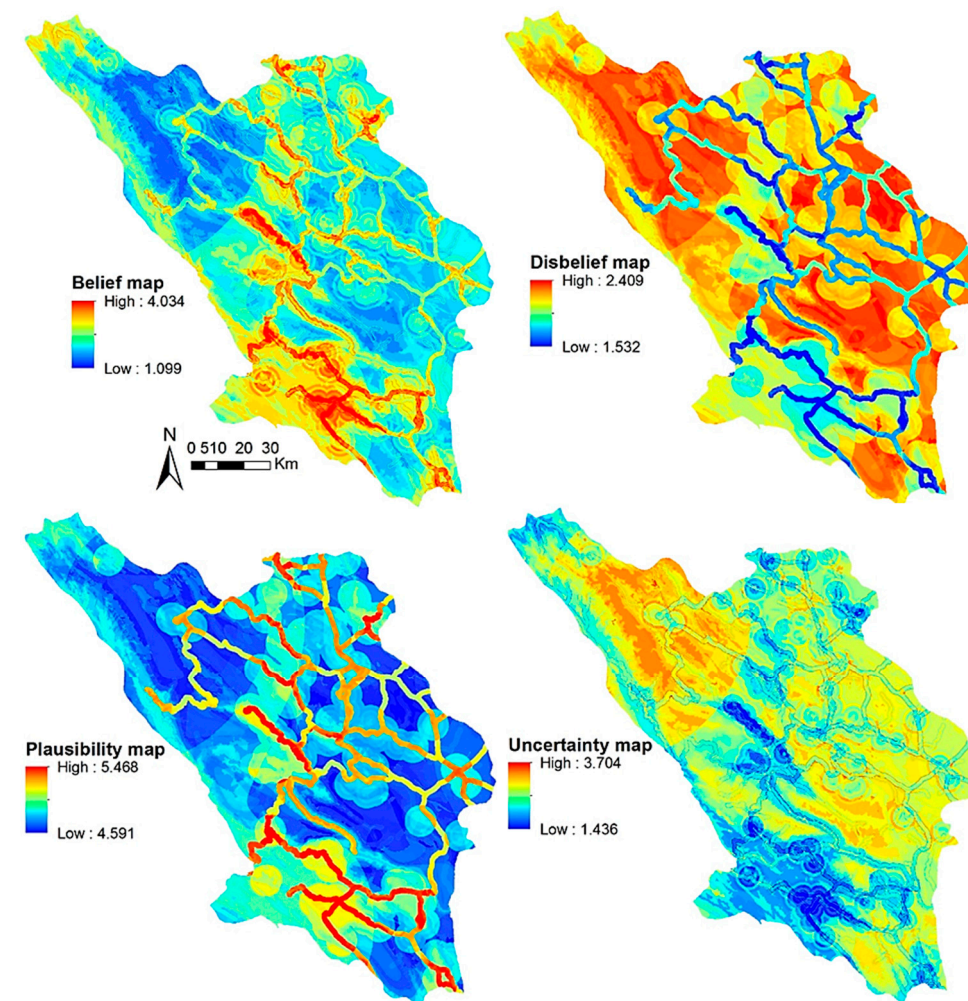


**Figure 5.** The index maps of the four probability mass functions of the EBF model.

The model parameters resulting from the application of the LR model are shown in Table 2. The final LR model for the training dataset retained only five (i.e., slope, rainfall, land use, and distance to populated areas and roads) of the twelve original variables (Table 3). The regression coefficient ( $\beta$ ) of the selected variables indicate the magnitude to which these variables exert an effect on the probability of wildfire occurrences in the research landscape; chief among them was the land use variable. This variable was used here as a proxy for human influences on the spatial pattern of wildfire probabilities [2,7,11,20,21] that delineated zones of similar conditions in terms of human-ignition patterns, indicating that dry farmlands and forests are the most susceptible portions of the landscape to fire occurrences. During field surveys, we found that while human activities predominantly controlled the distribution of all fires throughout the landscape, the type and contiguous patches of vegetation (i.e., fuel sources for fires) mainly determined the incidence of the largest fires.

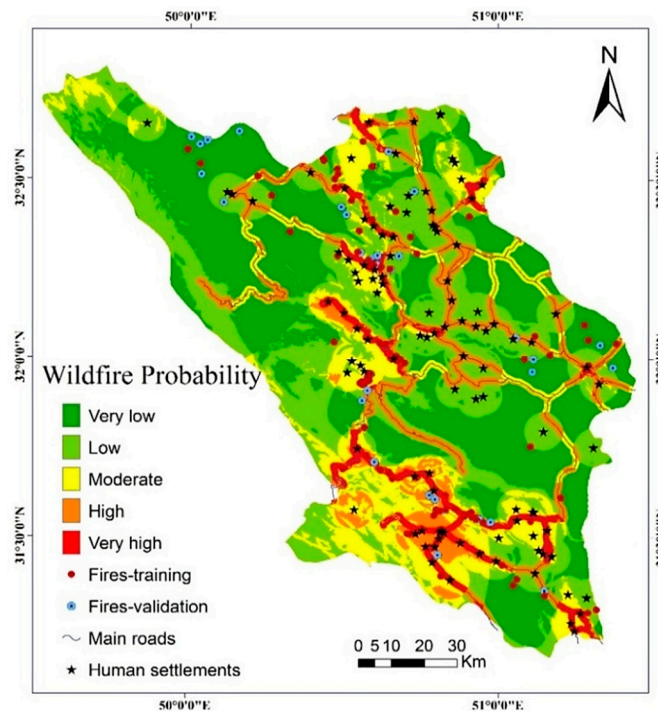


**Figure 6.** The distribution map of wildfire probability produced using the EBF model.

**Table 2.** Summary of the implementation of the logistic regression (LR) model.

Step	Chi-Square	−2 Log Likelihood	Cox & Snell R Square	Nagelkerke R Square
1	2.532	240.749a	0.075	0.100
2	7.617	235.434a	0.101	0.135
3	15.880	224.975a	0.151	0.201
4	13.302	220.813a	0.170	0.227
5	16.484	215.842b	0.192	0.256

a. Estimation terminated at iteration number 4 because parameter estimates changed by less than 0.001. b. Estimation terminated at iteration number 5 because parameter estimates changed by less than 0.001.

**Table 3.** Variable coefficients extracted using the LR model.

95% C.I. for EXP(B)		Exp (ß)	Sig.	df	Wald	S.E	ß	Variables in the Equation	
Upper	Lower								
0.897	0.373	0.579	0.14	1	5.979	0.224	−0.547	Slope	Step 5
0.932	0.454	0.650	0.019	1	5.497	0.183	0.430	Rainfall	
0.589	0.032	0.137	0.008	1	7.113	0.745	−1.990	Land use (Farmland)	
25.499	0.009	0.475	0.714	1	0.134	2.032	−0.744	Land use (Orchard)	
5.442	0.926	2.245	0.703	1	3.206	0.452	0.809	Land use (Dry farming)	
5.050	0.942	2.182	0.069	1	3.317	0.428	0.780	Land use (Forest)	
0.977	0.667	0.807	0.028	1	4.828	0.097	−0.214	Dis. to populated areas	
0.896	0.534	0.691	0.005	1	7.814	0.132	−0.369	Dis. to roads	
		165.936	0.000	1	20.194	1.137	−5.112	Constant	

S.E: Standard Error of estimate; Wald: Wald chi-square values; df: Degree of freedom; Sig: Significance value.

The negative coefficients for the slope and distance factors indicate that these variables are of little importance for the probability of fire occurrence (Table 3). Using these coefficients and Equation (7), the wildfire probability values for the entire study region were generated as follows:

$$Y = ((-5.112) + (\text{Slope} \times -0.547) + (\text{Rainfall} \times 0.430) + (\text{Farmland} \times -1.990) + (\text{Orchard} \times -0.744) + (\text{Dry farming} \times 0.809) + (\text{Forest} \times 0.780) + (\text{Distance to populated areas} \times -0.214) + (\text{Distance to roads} \times -0.369)) \quad (9)$$

Figure 7 shows the observed groups (1 (non-fire) and 2 (fire)) and the predicted probabilities of the pixels used in the LR model. The appropriate bunching of the observations towards the left and right ends of the graph demonstrates that the LR model performed reasonably well at classifying the training dataset into fires and non-fires. The final LR map of wildfire probability was developed by transferring the probability values to the ArcGIS software (Figure 8).

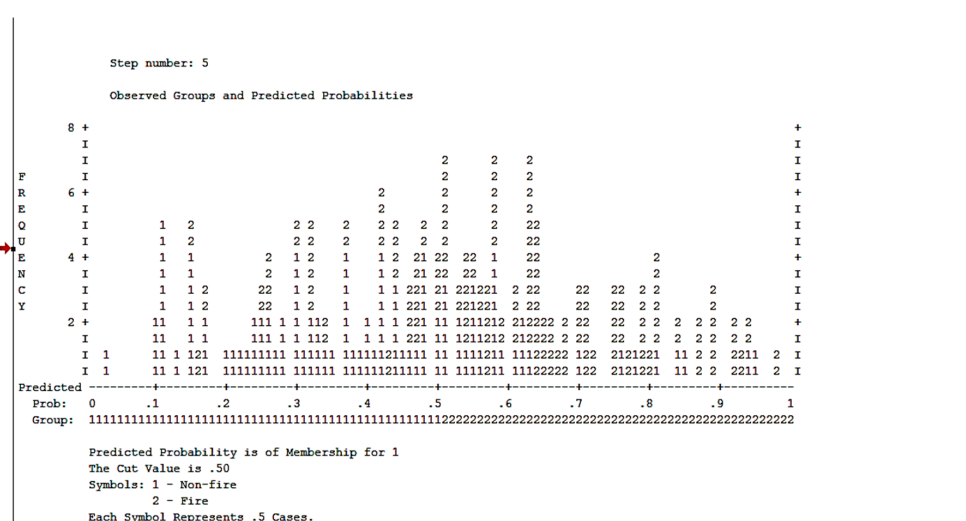


**Figure 7.** Observed groups and predicted probabilities extracted using the LR model.

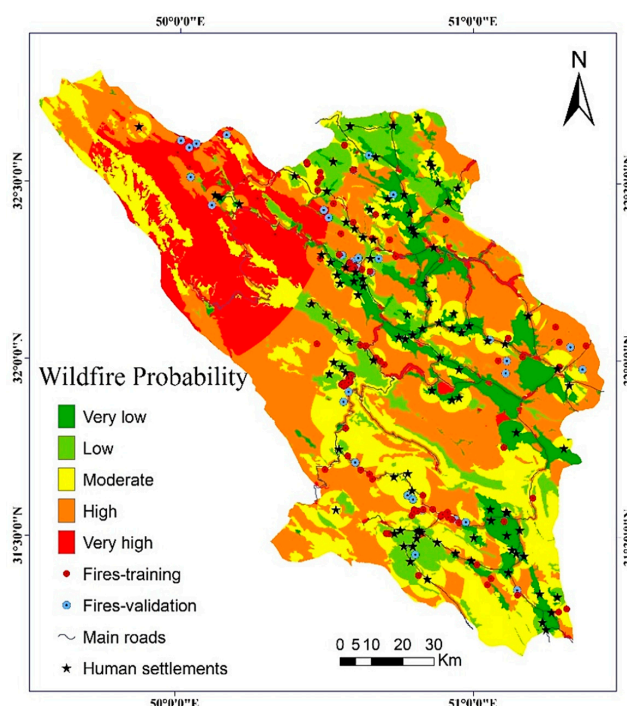


**Figure 8.** The distribution map of wildfire probability produced using the LR model.



Upon producing the wildfire probability maps using the EBF and LR models, the two maps were combined to achieve an ensemble map of wildfire probability (Figure 9). This operation resulted in combining characteristics for EBF and LR maps into a single probability map.

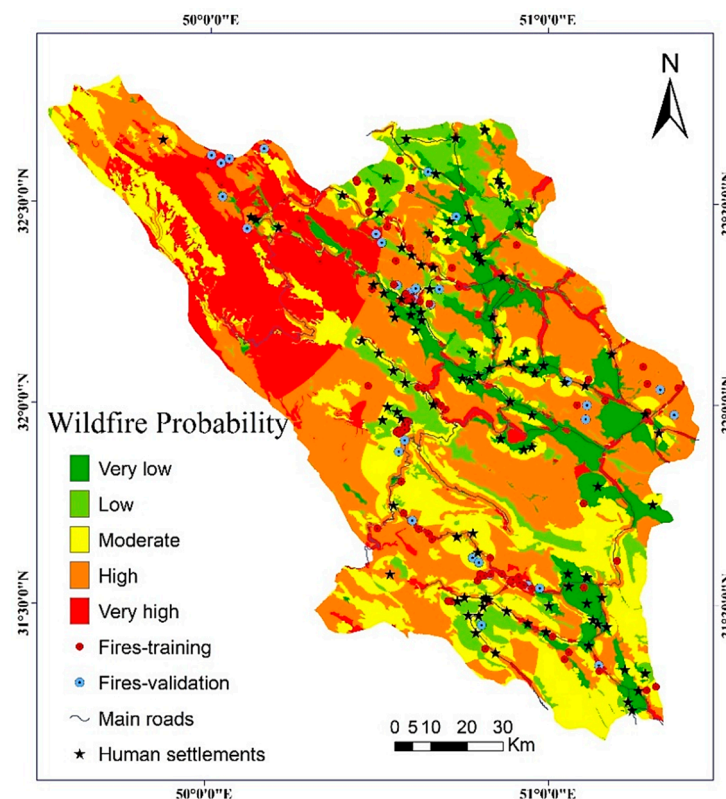


**Figure 9.** The ensemble (EBF-LR) wildfire probability map.

#### 4.3. Validation and Comparison

The three wildfire probability maps produced by the three models were compared using the success rates (Figure 10) and prediction rates (Figure 11). In the case of the EBF and LR models, LR showed the greatest goodness-of-fit with the training dataset (AUC = 0.843) and the capability to predict future fires (AUC = 0.728). In the literature, EBF and LR models were used either separately [20] or compared to other models [17]. While the EBF model proved itself to be rather simple and easy to apply [20], the LR model appears more complex, as this model requires the modelers to convert the data from the GIS standard format to the format required by the statistical software [17,21]. However, despite the LR that accepts both discrete and continuous inputs, EBF only operates on discrete-form inputs.

Applying the ensemble approach, we achieved an improved model performance in both training (AUC = 0.898) and validation (AUC = 0.864) datasets compared to those obtained using the LR and EBF models. The capability of hybrid and ensemble approaches for improving the predictive accuracy of natural phenomena has been widely acknowledged in previous works [16,35,36,39]. In a recent work, Hong et al. [21] proposed an integrated model that relied on the weight of evidence and the analytical hierarchy process and demonstrated a significantly improved prediction of future fires. The ensemble wildfire probability map developed in this study takes the advantages of both LR and EBF models that successfully measured the importance of each variable and its categories.

The results of the comparison of the success rates using the WSRT (Table 4) indicate that the training performance of the models differed significantly, as z- and p-values for the pairwise comparisons exceeded the critical values. Additionally, the same results were achieved by comparing the prediction rates (Table 5), indicating that the capability of the models to predict wildfires differed

significantly. While the EBF model can adequately explore the spatial associations between a variables class and past wildfires, the model fails to rank the variables and generally assumes equal weights for all variables [20]. This is due to the general philosophy of a bivariate model that investigates the significance of several variables separately [16].

Although in this study the multivariate LR model performed much better than the bivariate EBF model, LR has been frequently criticized due to its basic algorithm that considers a linear relationship between a phenomenon and its causal factors [21,34] that actually does not meet the complex nature of natural hazards [16,39]. In this context, some studies even suggest that the LR model tends to underestimate the probability of occurrence of an event [40]. However, some other studies demonstrated that the bivariate models are highly sensitive to the quality of input data and often fail to fully explore the real relationships between wildfires and their drivers [7,20]. On the other hand, some researchers believe that different methods have their own intrinsic advantages and disadvantages and it is not true that a single model is absolutely superior to the others [14,41].

With the increasing frequency and intensity of wildfires, it becomes more and more important to build and suggest accurate predictive models. Approaches integrating multiple individual models can provide robust estimates of future fires [16,21,24]. Given the proven capability of the ensemble approach adopted in this study, we can conclude that the single application of bivariate and multivariate models is inefficient and outdated, highlighting the need to update their basic structures toward an advanced model. Thus, in line with the efforts devoted to developing new models for the prediction of landslides [39] and floods [42], further research is needed to improve the wildfire prediction models and the ability of managers and authorities for making more informed fire presentation and suppression decisions.

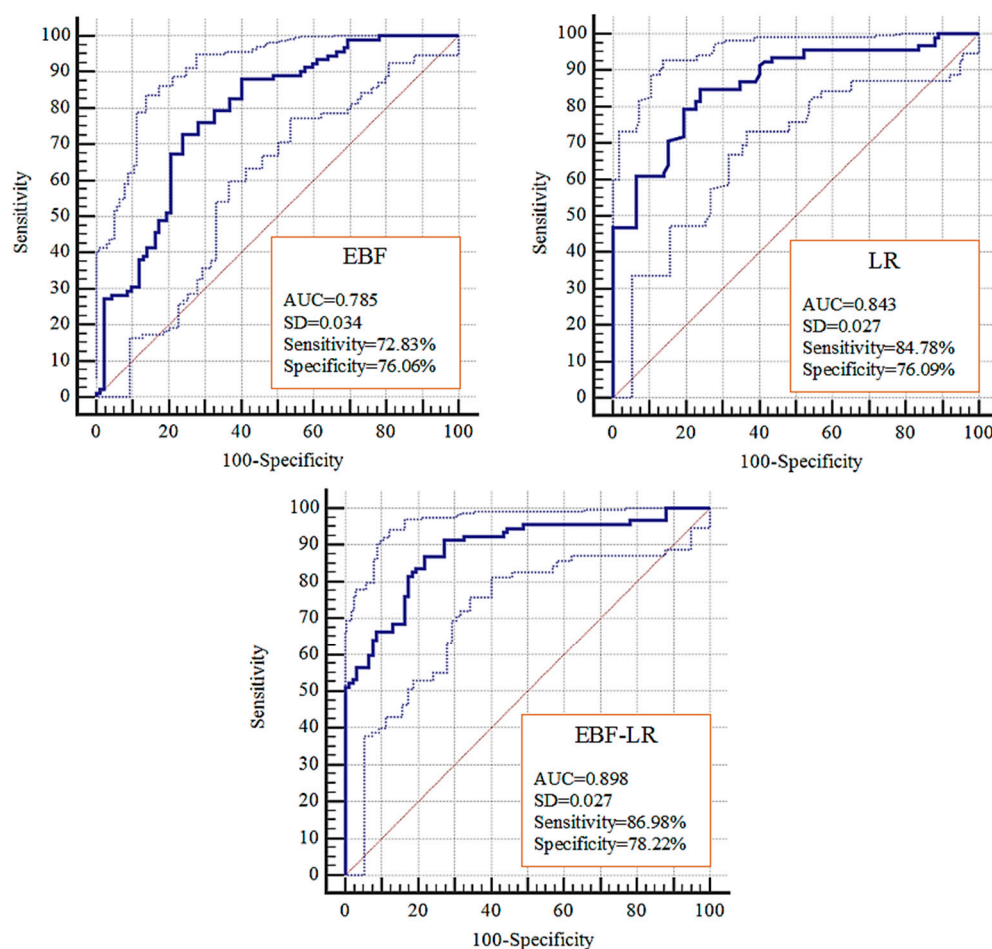


Figure 10. Success rate curves of the three models.

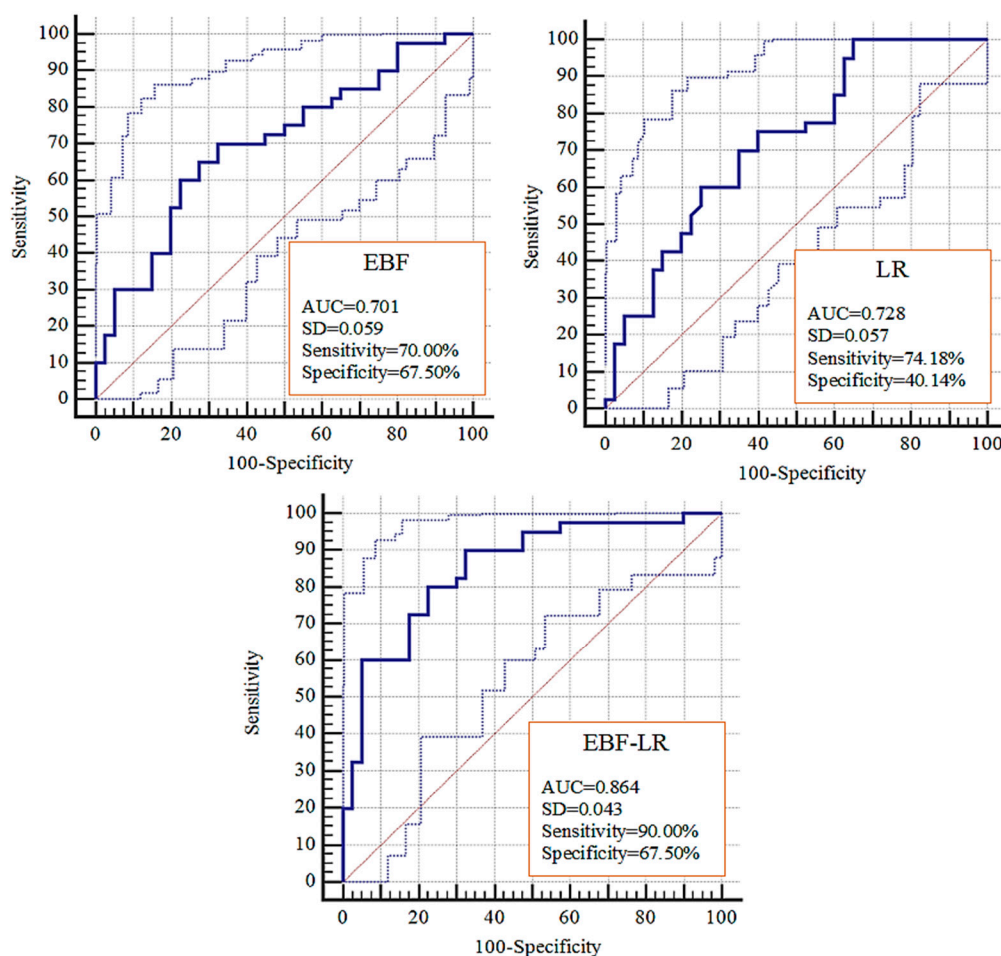


Figure 11. Prediction rate curves of the three models.

Table 4. Pairwise comparison of the models' success rates using the Wilcoxon Signed-Rank Test (WSRT).

	z-Value	p-Value	Sig.
EBF vs. LR	11.463	$p < 0.0001$	Yes
EBF vs. EBF-LR	−11.763	$p < 0.0001$	Yes
LR vs. EBF-LR	−11.764	$p < 0.0001$	Yes

Table 5. Pairwise comparison of the models' prediction rates using the WSRT.

	z-Value	p-Value	Sig.
EBF vs. LR	7.770	$p < 0.0001$	Yes
EBF vs. EBF-LR	−7.769	$p < 0.0001$	Yes
LR vs. EBF-LR	7.347	$p < 0.0001$	Yes

## 5. Conclusions

With in this paper, we presented a comparison of the EBF and LR models for mapping wildfire probability and focused on their predictive capabilities, which is often regarded as the main part of a predictive modeling effort. Whereas the bivariate EBF model successfully identified the variable classes that contribute the most to fire ignition, the multivariate LR model enabled us to rank the explanatory variables with the most influence. The validation process demonstrated the supremacy of the LR model, which provided a more accurate prediction of future fires and their spatial distributions. The difference between the two models motivated us to take an ensemble approach to our modeling process. We used this approach to check for a possible improvement in the results by

combining two probability maps. The results of this map combination clearly revealed that the EBF and LR models act very well in conjunction with each other and can significantly improve the ability to predict future wildfires. More generally, further research is required to understand the nature of different models and to understand what characteristics motivate modelers to select a model or not. Understanding these characteristics can help modelers and managers in ways that provide an accurate estimate of wildfire probability in reasonable computation time. Future research must provide explicit information about model selection based on predictive capability, ideally using a more inclusive range of independent variables and powerful data collection methods that will capture landscape characteristics realistically.

**Author Contributions:** Conceptualization, A.J. and D.M.-G.; data acquisition, D.M.-G.; methodology, A.J., D.M.-G., B.T.P., and D.T.B.; writing—original draft preparation, A.J.; writing—review and editing, A.J., D.M.-G., B.T.P., and D.T.B.; APC, B.T.P. and D.T.B.

**Funding:** This research was partially funded by University of South-Eastern Norway.

**Conflicts of Interest:** The authors declare no conflict of interest.

## References

1. Pacheco, A.P.; Claro, J.; Fernandes, P.M.; de Neufville, R.; Oliveira, T.M.; Borges, J.G.; Rodrigues, J.C. Cohesive fire management with in an uncertain environment: A review of risk handling and decision support systems. *Ecol. Manag.* **2015**, *347*, 1–17. [[CrossRef](#)]
2. Pourtaghi, Z.S.; Pourghasemi, H.R.; Aretano, R.; Semeraro, T. Investigation of general indicators influencing on forest fire and its susceptibility modeling using different data mining techniques. *Ecol. Indic.* **2016**, *64*, 72–84. [[CrossRef](#)]
3. Bowman, D.M.; Balch, J.K.; Artaxo, P.; Bond, W.J.; Carlson, J.M.; Cochrane, M.A.; D’Antonio, C.M.; De Fries, R.S.; Doyle, J.C.; et al. Fire in the Earth system. *Science* **2009**, *324*, 481–484. [[CrossRef](#)] [[PubMed](#)]
4. Meng, Y.; Deng, Y.; Shi, P. Mapping Forest Wildfire Risk of the World. In *World Atlas of Natural Disaster Risk*; Springer: Berlin/Heidelberg, Germany, 2015; pp. 261–275.
5. Calder, W.J.; Shuman, B. Extensive wildfires, climate change, and an abrupt state change in subalpine ribbon forests, Colorado. *Ecology* **2017**, *98*, 2585–2600. [[CrossRef](#)]
6. Stevens-Rumann, C.S.; Kemp, K.B.; Higuera, P.E.; Harvey, B.J.; Rother, M.T.; Donato, D.C.; Morgan, P.; Veblen, T.T. Evidence for declining forest resilience to wildfires under climate change. *Ecol. Lett.* **2018**, *21*, 243–252. [[CrossRef](#)] [[PubMed](#)]
7. Jaafari, A.; Mafi-Gholami, D.; Zenner, E.K. A Bayesian modeling of wildfire probability in the Zagros Mountains, Iran. *Ecol. Inf.* **2017**, *39*, 32–44. [[CrossRef](#)]
8. Petty, A.M.; Isendahl, C.; Brenkert-Smith, H.; Goldstein, D.J.; Rhemtulla, J.M.; Rahman, S.A.; Kumasi, T.C. Applying historical ecology to natural resource management institutions: Lessons from two case studies of landscape fire management. *Glob. Environ. Chang.* **2015**, *31*, 1–10. [[CrossRef](#)]
9. Pettit, N.E.; Naiman, R.J.; Warfe, D.M.; Jardine, T.D.; Douglas, M.M.; Bunn, S.E.; Davies, P.M. Productivity and connectivity in tropical riverscapes of northern Australia: Ecological insights for management. *Ecosystems* **2017**, *20*, 492–514. [[CrossRef](#)]
10. Monedero, S.; Ramirez, J.; Cardil, A. Predicting fire spread and behaviour on the fireline. Wildfire analyst pocket: A mobile app for wildland fire prediction. *Ecol. Model.* **2019**, *392*, 103–107. [[CrossRef](#)]
11. Ngoc-Thach, N.; Ngo, D.B.T.; Xuan-Canh, P.; Hong-Thi, N.; Thi, B.H.; NhatDuc, H.; Dieu, T.B. Spatial pattern assessment of tropical forest fire danger at Thuan Chau area (Vietnam) using GIS-based advanced machine learning algorithms: A comparative study. *Ecol. Inf.* **2018**, *48*, 74–85. [[CrossRef](#)]
12. Chuvieco, E.; Congalton, R.G. Application of remote sensing and geographic information systems to forest fire hazard mapping. *Rem. Sens. Env.* **1989**, *29*, 147–159. [[CrossRef](#)]
13. De Vliegheer, B.M. Risk assessment for environmental degradation caused by fires using remote sensing and GIS in a Mediterranean Region (South-Euboea, Central Greece). In *Proceedings of the International IGARSS’92 Geoscience and Remote Sensing Symposium*, Houston, TX, USA, 26–29 May 1992; Volume 1, pp. 44–47.



14. Jaafari, A.; Zenner, E.K.; Pham, B.T. Wildfire spatial pattern analysis in the Zagros Mountains, Iran: A comparative study of decision tree based classifiers. *Ecol. Inf.* **2018**, *43*, 200–211. [\[CrossRef\]](#)
15. Tien Bui, D.; Le, K.T.T.; Nguyen, V.C.; Le, H.D.; Revhaug, I. Tropical forest fire susceptibility mapping at the cat Ba national park area, Hai Phong city, Vietnam, using GIS-Based kernel logistic regression. *Remote Sens.* **2016**, *8*, 347. [\[CrossRef\]](#)
16. Jaafari, A.; Zenner, E.K.; Panahi, M.; Shahabi, H. Hybrid artificial intelligence models based on a neuro-fuzzy system and metaheuristic optimization algorithms for spatial prediction of wildfire probability. *Agric. For. Meteorol.* **2019**, *266*, 198–207. [\[CrossRef\]](#)
17. Pourghasemi, H.R. GIS-based forest fire susceptibility mapping in Iran: A comparison between evidential belief function and binary logistic regression models. *Scand. J. For. Res.* **2016**, *31*, 80–98. [\[CrossRef\]](#)
18. Pourtaghi, Z.S.; Pourghasemi, H.R.; Rossi, M. Forest fire susceptibility mapping in the Minudasht forests, Golestan province, Iran. *Environ. Earth Sci.* **2015**, *73*, 1515–1533. [\[CrossRef\]](#)
19. Hong, H.; Naghibi, S.A.; Dashtpaderdi, M.M.; Pourghasemi, H.R.; Chen, W. A comparative assessment between linear and quadratic discriminant analyses (LDA-QDA) with frequency ratio and weights-of-evidence models for forest fire susceptibility mapping in China. *Arab. J. Geosci.* **2017**, *10*, 167. [\[CrossRef\]](#)
20. Nami, M.H.; Jaafari, A.; Fallah, M.; Nabiuni, S. Spatial prediction of wildfire probability in the Hyrcanian ecoregion using evidential belief function model and GIS. *Int. J. Environ. Sci. Technol.* **2018**, *15*, 373–384. [\[CrossRef\]](#)
21. Hong, H.; Jaafari, A.; Zenner, E.K. Predicting spatial patterns of wildfire susceptibility in the Huichang County, China: An integrated model to analysis of landscape indicators. *Ecol. Indic.* **2019**, *101*, 878–891. [\[CrossRef\]](#)
22. Umar, Z.; Pradhan, B.; Ahmad, A.; Jebur, M.N.; Tehrany, M.S. Earthquake induced landslide susceptibility mapping using an integrated ensemble frequency ratio and logistic regression models in West Sumatera Province, Indonesia. *Catena* **2015**, *118*, 124–135. [\[CrossRef\]](#)
23. Chen, W.; Sun, Z.; Han, J. Landslide susceptibility modeling using integrated ensemble weights of evidence with logistic regression and random forest models. *Appl. Sci.* **2019**, *9*, 171. [\[CrossRef\]](#)
24. Tien Bui, D.; Bui, Q.T.; Nguyen, Q.P.; Pradhan, B.; Nampak, H.; Trinh, P.T. A hybrid artificial intelligence approach using GIS-based neural-fuzzy inference system and particle swarm optimization for forest fire susceptibility modeling at a tropical area. *Agric. For. Meteorol.* **2017**, *233*, 32–44. [\[CrossRef\]](#)
25. Jaafari, A.; Pourghasemi, H.R. Factors Influencing Regional Scale Wildfire Probability in Iran: An Application of Random Forest and Support Vector Machine. In *Modeling in GIS and R for Earth and Environmental Science*; Pourghasemi, H.R., Candan, G., Eds.; Elsevier: Amsterdam, The Netherlands, 2019.
26. Tehrany, M.S.; Kumar, L. The application of a Dempster–Shafer-based evidential belief function in flood susceptibility mapping and comparison with frequency ratio and logistic regression methods. *Environ. Earth Sci.* **2018**, *77*, 490. [\[CrossRef\]](#)
27. Dempster, A.P. Upper and lower probabilities induced by a multivalued mapping. *Ann. Math. Stat.* **1967**, *38*, 325–339. [\[CrossRef\]](#)
28. Dempster, A.P. Upper and lower probability inferences based on a sample from a finite univariate population. *Biometrika* **1967**, *54*, 515–528. [\[CrossRef\]](#) [\[PubMed\]](#)
29. Shafer, G.A. *Mathematical Theory of Evidence*; Princeton University Press: Princeton, NJ, USA, 1976; 297p.
30. Carranza, E.J.M.; Van Ruitenbeek, F.; Hecker, C.; van der Meijde, M.; van der Meer, F.D. Knowledge-guided data-driven evidential belief modeling of mineral prospectivity in Cabo de Gata, SE Spain. *Int. J. Appl. Earth Obs.* **2008**, *10*, 374–387. [\[CrossRef\]](#)
31. Naghibi, S.A.; Pourghasemi, H.R.; Dixon, B. GIS-based groundwater potential mapping using boosted regression tree, classification and regression tree, and random forest machine learning models in Iran. *Environ. Monit. Assess.* **2016**, *188*, 1–27. [\[CrossRef\]](#) [\[PubMed\]](#)
32. Carranza, E.J.M.; Woldai, T.; Chikambwe, E.M. Application of data-driven evidential belief functions to prospectivity mapping for aquamarine-bearing pegmatites, Lundazi district, Zambia. *Nat. Resour. Res.* **2005**, *14*, 47–63. [\[CrossRef\]](#)
33. Gorum, T.; Carranza, E.J.M. Control of style-of-faulting on spatial pattern of earthquake-triggered landslides. *Int. J. Environ. Sci. Technol.* **2015**, *12*, 3189–3212. [\[CrossRef\]](#)
34. Pham, B.T.; Prakash, I.; Jaafari, A.; Bui, D.T. Spatial prediction of rainfall-induced landslides using aggregating one-dependence estimators classifier. *J. Ind. Soc. Remote Sens.* **2018**, *46*, 1457–1470. [\[CrossRef\]](#)

35. Choubin, B.; Moradi, E.; Golshan, M.; Adamowski, J.; Sajedi-Hosseini, F.; Mosavi, A. An Ensemble prediction of flood susceptibility using multivariate discriminant analysis, classification and regression trees, and support vector machines. *Sci. Total. Environ.* **2019**, *651*, 2087–2096. [[CrossRef](#)] [[PubMed](#)]
36. Jaafari, A. LiDAR-supported prediction of slope failures using an integrated ensemble weights-of-evidence and analytical hierarchy process. *Environ. Earth Sci.* **2018**, *77*, 42. [[CrossRef](#)]
37. Hanley, J.A.; McNeil, B.J. The meaning and use of the area under a receiver operating characteristic (ROC) curve. *Radiology* **1982**, *143*, 29–36. [[CrossRef](#)] [[PubMed](#)]
38. Wilcoxon, F. Individual comparisons by ranking methods. *Biom. Bull.* **1945**, *1*, 80–83. [[CrossRef](#)]
39. Jaafari, A.; Panahi, M.; Pham, B.T.; Shahabi, H.; Bui, D.T.; Rezaie, F.; Lee, S. Meta optimization of an adaptive neuro-fuzzy inference system with grey wolf optimizer and biogeography-based optimization algorithms for spatial prediction of landslide susceptibility. *Catena* **2019**, *175*, 430–445. [[CrossRef](#)]
40. Zhu, A.X.; Miao, Y.; Wang, R.; Zhu, T.; Deng, Y.; Liu, J.; Yang, L.; Cheng-Zhi, Q.; Hong, H. A comparative study of an expert knowledge-based model and two data-driven models for landslide susceptibility mapping. *Catena* **2018**, *166*, 317–327. [[CrossRef](#)]
41. Tutmez, B.; Ozdogan, M.G.; Boran, A. Mapping forest fires by nonparametric clustering analysis. *J. For. Res.* **2018**, *29*, 177–185. [[CrossRef](#)]
42. Termeh, S.V.R.; Kornejady, A.; Pourghasemi, H.R.; Keesstra, S. Flood susceptibility mapping using novel ensembles of adaptive neuro fuzzy inference system and metaheuristic algorithms. *Sci. Total Environ.* **2018**, *615*, 438–451. [[CrossRef](#)]



© 2019 by the authors. Licensee MDPI, Basel, Switzerland. This article is an open access article distributed under the terms and conditions of the Creative Commons Attribution (CC BY) license (<http://creativecommons.org/licenses/by/4.0/>).